4446 *Chem. Mater.* **2010,** *22,* 4446–4454
DOI:10.1021/cm101138h

CHEMISTRY OF MATERIALS
Article

Syntheses and Characterization of Wurtzite CoO, Rocksalt CoO, and Spinel Co_3O_4 Nanocrystals: Their Interconversion and Tuning of Phase and Morphology

Ki Min Nam,[†] Jae Ha Shim,[†] Dong-Wook Han,[§] Hyuk Sang Kwon,[§] Yong-Mook Kang,[∥] Yan Li,[‡] Hyunjoon Song,[†] Won Seok Seo,*[,‡] and Joon T. Park*[,†]

[†]*Department of Chemistry, Korea Advanced Institute of Science and Technology (KAIST), Daejeon, 305-701, Korea,* [‡]*Department of Chemistry, Inorganic and Bio-Materials Center of BK21, Sogang University, Seoul, 121-742, Korea,* [§]*Department of Materials Science and Engineering, Korea Advanced Institute of Science and Technology (KAIST), Daejeon, 305-701, Korea, and* [∥]*Division of Advanced Materials Engineering, Kongju National University, 275 Budae-dong, Cheonan, Chungnam, Korea*

Received April 23, 2010. Revised Manuscript Received June 23, 2010

Pure rocksalt (c-CoO) and wurtzite (h-CoO) phases of cobaltous oxide (CoO) have been selectively prepared through thermodynamically and kinetically controlled reactions of a single molecular precursor $Co(acac)_3$ (acac: acetylacetonate), respectively. Changing thermal decomposition conditions of the precursor produces different phases and distinct morphologies of the cobaltous oxides. Hexagonal pyramidal shaped h-CoO nanocrystals have been formed by a flash heating of the reaction mixture (185 °C for 2 h, kinetic control condition), whereas cube shaped c-CoO nanocrystals have been produced by a prolonged heating at a relatively low temperature (130 °C for 12 h, thermodynamic control condition). Addition of o-Dichlorobenzene (o-DCB) to the reaction mixture alters the reaction condition to the thermodynamic control regime by slowing down the decomposition rate of the precursor. Further increase of the concentration of o-DCB in the reaction mixture changes the morphology of product from h-CoO hexagonal pyramids to h-CoO nanorods with various aspect ratios and finally to c-CoO nanocrystals. Air oxidation at 240 °C for 5 h of either h-CoO or c-CoO nanocrystals yields spinel Co_3O_4 nanocrystals with retention of the original crystal morphology. During the oxidation process, the h-CoO phase has been converted into Co_3O_4 via formation of the c-CoO phase, but the c-CoO phase has been directly oxidized to Co_3O_4. The electrochemical properties of the h-CoO, c-CoO, and spinel Co_3O_4 nanocrystals toward lithium exhibit characteristic features reflecting their Gibbs free energies. This work allows understanding of the detailed mechanism and energetics of selective formation, phase transformation, morphology control, and electrochemical properties in the closely related nanostructured cobalt oxides.

Introduction

Transition metal oxides are an important group of materials because they form a wide variety of structures, display many interesting properties, and have numerous applications.[1−4] In particular, cobalt oxides have attracted great interest in their potential applications as catalysts, magnetic data storage devices, lithium-ion battery materials, and solid-state sensors[5−9] because of their chemical stability and magnetic properties. Cobaltous oxide typically crystallizes in two stable phases, cubic rocksalt CoO (c-CoO, space group $Fm3m$) with octahedral Co^{2+} and hexagonal wurtzite CoO (h-CoO, space group $P6_3mc$) with tetrahedral Co^{2+} ions.[10] Numerous preparation methods of c-CoO have been reported, but the majority of the synthetic processes are based on thermal decomposition of cobalt precursors in hydrocarbon solvents.[11−18] For example, Yin and Wang reported

*To whom correspondence should be addressed. E-mail: joontpark@kaist.ac.kr (J.T.P.), wsseo@sogang.ac.kr (W.S.S.).

(1) Wang, Z. L.; Song, J. *Science* **2006**, *312*, 242–246.
(2) Subramanian, V.; Wolf, E. E.; Kamat, P. V. *J. Am. Chem. Soc.* **2004**, *126*, 4943–4950.
(3) Seo, W. S.; Jo, H. H.; Lee, K.; Kim, B.; Oh, S. J.; Park, J. T. *Angew. Chem., Int. Ed.* **2004**, *43*, 1115–1117.
(4) Cheng, K.; Peng, S.; Sun, S. *J. Am. Chem. Soc.* **2009**, *131*, 10637–10644.
(5) Li, W.-Y.; Xu, L.-N.; Chen, J. *Adv. Funct. Mater.* **2005**, *15*, 851–857.
(6) Wang, G.; Shen, X.; Horvat, J.; Wang, B.; Liu, H.; Wexler, D.; Yao, J. *J. Phys. Chem. C* **2009**, *113*, 4357–4361.
(7) Binotto, G.; Larcher, D.; Prakash, A. S.; Urbina, R. H.; Hegde, M. S.; Tarascon, J.-M. *Chem. Mater.* **2007**, *19*, 3032–3040.
(8) Choi, H. C.; Lee, S. Y.; Kim, S. B.; Kim, M. G.; Lee, M. K.; Shin, H. J.; Lee, J. S. *J. Phys. Chem. B* **2002**, *103*, 9252–9260.
(9) Nam, H.-J.; Sasaki, T.; Koshizaki, N. *J. Phys. Chem. B* **2006**, *110*, 23081–238084.
(10) Seo, W. S.; Shim, J. H.; Oh, S. J.; Lee, E. K.; Hur, N. H.; Park, J. T. *J. Am. Chem. Soc.* **2005**, *127*, 6188–6189.
(11) Yin, J. S.; Wang, Z. L. *J. Phys. Chem. B* **1997**, *101*, 8979–8983.
(12) Ghosh, M.; Sampathkumaran, E. V.; Rao, C. N. R. *Chem. Mater.* **2005**, *17*, 2348–2352.
(13) Zhang, Y.; Zhu, J.; Song, X.; Zhong, X. *J. Phys. Chem. C* **2008**, *112*, 5322–5327.
(14) Risbud, A. S.; Snedeker, L. P.; Elcombe, M. M.; Cheetham, A. K.; Seshadri, R. *Chem. Mater.* **2005**, *17*, 834–838.
(15) Park, J.; An, K.; Hwang, Y.; Park, J.-G.; Noh, H.-J.; Kim, J.-Y.; Park, J.-H.; Hwang, N.-M.; Hyeon, T. *Nat. Mater.* **2004**, *3*, 891–895.
(16) An, K.; Lee, N.; Park, J.; Kim, S. C.; Hwang, Y.; Park, J.-G.; Kim, J.-Y.; Park, J.-H.; Han, M. J.; Yu, J.; Hyeon, T. *J. Am. Chem. Soc.* **2006**, *128*, 9753–9760.

 Published on Web 07/13/2010

synthesis of c-CoO nanocrystals with tetrahedral shapes by oxidation of $Co_2(CO)_8$ in toluene in the presence of sodium bis(2-ethylhexyl) sulfosuccinate at 130 °C.[11] Rao and co-workers synthesized c-CoO nanoparticles sized 4.5−18 nm by Co(II) cupferronate decomposition in decaline under solvothermal conditions.[12] Zhong and co-workers obtained a series of c-CoO nanocrystals with various morphologies and sizes via decomposition of Co(II)-oleate complex at 280−320 °C.[13] However, h-CoO nanocrystals have not been fully characterized before our work,[10] which has been reported in a preliminary form. ZnO is the only stable metal oxide previously discovered to possess such a hexagonal structure. Seshadri et al. reported a synthetic approach to nearly pure wurtzite CoO by decomposition of $Co(acac)_2$ simultaneously with our preliminary account.[14] Hyeon and co-workers mentioned that h-CoO nanorods formed in a short pencil shape under thermal decomposition of a Co(II)-oleate complex during their study for wide applicability of syntheses of transition metal oxides from the thermolysis of metal-oleate complexes,[15] which was fully characterized afterward.[16] Liu et al. followed our synthetic procedures and studied the hexagonal-to-cubic transformation in the nanocrystalline CoO.[18] However, the formation mechanism and correlation between crystallographic structure and formation kinetics of cobalt oxides have not been clearly explored as of yet.

In addition to CoO, Co_3O_4 has been a central issue because of its superior magnetic, catalytic, and electrochemical features. Co_3O_4 has a normal spinel structure (space group *Fd*3*m*) in which Co^{2+} and Co^{3+} ions are at the centers of tetrahedral and octahedral sites, respectively. Various Co_3O_4 morphologies, including particles, wires, and fibers, have been fabricated in nanometer scales.[19−22] Most Co_3O_4 nanostructures have been prepared using thermal decomposition of cobalt salts and organocobalt precursors.[19,20] Direct oxidation of CoO nanocrystals, however, has not been reported for the preparation of Co_3O_4.

The detailed transformation mechanism among various cobalt oxides is important in understanding the lattice structure and morphological effect in compositionally closed systems. Chemical and electrochemical properties of the three cobalt oxide phases are also very interesting issues. Cobalt oxides are known to exhibit superior electrochemical features as negative electrode materials in lithium ion batteries.[23−26] Interestingly, the mechanistic aspect of Li reactivity for the metal oxides involves the reduction and oxidation of small metal−metal oxide nanoparticles as well as the concomitant formation and decomposition of Li_2O, which differs from the classical Li insertion/extraction or Li-alloying/dealloying processes.[27,28] c-CoO is known to react reversibly with lithium through 2e reduction at a low voltage range as $CoO + 2Li^+ + 2e^- \leftrightarrow Co + Li_2O$ and spinel Co_3O_4 to react with more than eight lithium per formula unit down to 0.01 V.[23,24] However, the reactivity of h-CoO toward lithium and the comparison of relative chemical energies between different cobalt oxide phases have been unprecedented, although cobalt oxide systems are the most important and promising for anode materials of lithium ion batteries among transition metal oxides.

Herein we report a full account of syntheses and characterization of h-CoO and c-CoO nanocrystals with controlled morphologies of hexagonal pyramids, rods, and cubes in a selective manner. The hexagonal and cubic phases have been controlled by changing thermal decomposition kinetics of the cobalt precursor, $Co(acac)_3$ (acac = acetylacetonato), in benzylamine. Addition of o-DCB slows down the decomposition rates, and drives the reactions to the thermodynamic control regime. Moreover, air oxidation of both h-CoO and c-CoO nanocrystals have produced spinel Co_3O_4 nanocrystals with retention of the original morphology of CoO. The detailed crystal structures during oxidation reactions have been carefully examined. Finally, the electrochemical properties of h-CoO toward lithium have been investigated for the first time and compared with those of c-CoO and spinel Co_3O_4 to elucidate their relative electrochemical activities.

Experimental Section

General Methods. Synthesis of CoO nanocrystals was carried out using standard Schlenk techniques under an argon atmosphere. $Co(acac)_3$ (99.99+%, Sigma-Aldrich), benzylamine (99%, Sigma-Aldrich), and 1,2-dichlorobenzene (99%, Sigma-Aldrich) were used without further purification.

Preparation of h-CoO Hexagonal Pyramids. A green slurry of $Co(acac)_3$ (0.20 g, 0.56 mmol) and benzylamine (12.0 g, 112.0 mmol, 200 equiv) in a 100 mL Schlenk flask connected to a bubbler was vigorously stirred in a preheated oil bath at 185 °C. The reaction mixture was maintained at this temperature for 2 h, and the resulting green reaction mixture was cooled to room temperature. Toluene (10 mL) and ethanol (30 mL) were added to the green suspension, the suspension was centrifuged, and the supernatant was removed. The residue was washed with ethanol (30 mL × 3 times) to provide green h-CoO nanocrystals. The resulting nanocrystals are hexagonal pyramids with an average side edge length of 40 ± 6.4 nm and a basal edge length of 20 ± 5.0 nm.

Preparation of h-CoO Nanorods. A green slurry of $Co(acac)_3$ (0.20 g, 0.56 mmol) in benzylamine (6.02 g, 56.1 mmol, 100 equiv) and o-dichlorobenzene (6.60 g, 44.9 mmol, 80 equiv, 5:4 molar ratio of benzylamine: o-dichlorobenzene) was vigorously

(17) Zhang, Y.; Zhong, X.; Zhu, J.; Song, X. *Nanotechnology* **2007**, *18*, 195605.
(18) Liu, J. F.; Yin, S.; Wu, H. P.; Zeng, Y. W.; Hu, X. R.; Wang, Y. W.; Lv, G. L.; Jiang, J. Z. *J. Phys. Chem. B* **2006**, *110*, 21588–21592.
(19) He, T.; Chen, D.; Jiao, X. *Chem. Mater.* **2004**, *16*, 737–743.
(20) Jana, N. R.; Chen, Y.; Peng, X. *Chem. Mater.* **2004**, *16*, 3931–3935.
(21) Shi, X.; Han, S.; Sanedrin, R. J.; Galvez, C.; Ho, D. G.; Hernandez, B.; Zhou, F.; Selke, M. *Nano Lett.* **2002**, *2*, 289–293.
(22) Salabas, E. L.; Rumplecker, A.; Kleitz, F.; Radu, F.; Schuth, F. *Nano Lett.* **2006**, *6*, 2977–2981.
(23) Poizot, P.; Laruelle, S.; Grugeon, S.; Dupont, L.; Tarascon, J.-M. *Nature* **2000**, *407*, 496–499.
(24) Larcher, D.; Sudant, G.; Leriche, J.-B.; Chabre, Y.; Tarascon, J.-M. *J. Electrochem. Soc.* **2002**, *149*, A234–A241.
(25) Badway, F.; Plitz, I.; Grugeon, S.; Laruelle, S.; Dolle, M.; Gozdz, A. S.; Tarascon, J.-M. *Electrochem. Solid-State Lett.* **2002**, *5*, A115–A118.
(26) Dedryvere, R.; Laruelle, S.; Grugeon, S.; Poizot, P.; Gonbeau, D.; Tarascon, J.-M. *Chem. Mater.* **2004**, *16*, 1056–1061.
(27) Bruce, P. G.; Scrosati, B.; Tarascon, J.-M. *Angew. Chem., Int. Ed.* **2008**, *47*, 2930–2946.
(28) Jiang, C.; Hosono, E.; Zhou, H. *Nanotoday* **2006**, *1*, 28–33.

Scheme 1. Selective Formation of h-CoO, c-CoO Nanocrystals, and h-CoO Nanorods through the Kinetic versus Thermodynamic Reaction Control and the Effect of o-DCB

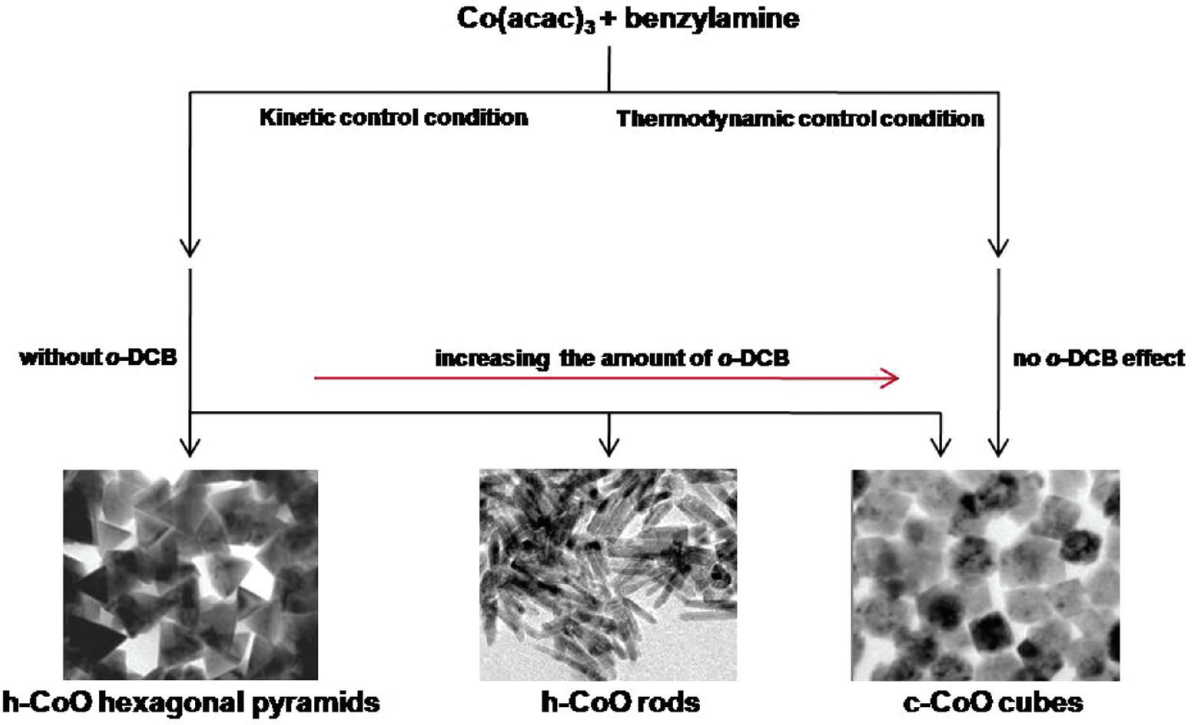

stirred in a preheated oil bath at 185 °C. The reaction mixture was maintained at this temperature for 2.5 h, and the resulting green reaction mixture was cooled to room temperature. A similar purification procedure to that listed above yielded h-CoO nanorods with an average width of 7 ± 0.9 nm and a length of 65 ± 9.8 nm. Analogous synthetic and purification procedures to those above afforded h-CoO nanorods with dimensions of 9 nm × 50 nm and 11 nm × 40 nm by employing 2:1 ratio of benzylamine (6.02 g, 56.1 mmol, 100 equiv) and o-dichlorobenzene (4.13 g, 28.1 mmol, 50 equiv), and 5:1 ratio of benzylamine (6.02 g, 56.1 mmol, 100 equiv) and o-dichlorobenzene (1.65 g, 11.2 mmol, 20 equiv), respectively.

Preparation of c-CoO Nanocrystals. Method 1: A green slurry of $Co(acac)_3$ (0.40 g, 1.12 mmol) in benzylamine (6.02 g, 56.1 mmol, 50 equiv) was vigorously stirred in a preheated oil bath at 130 °C for 12 h. The reaction mixture was further heated to 185 °C with a ramping rate of 10 °C/min and was maintained at this temperature for 2 h. Separation and purification procedures similar to those above yielded 38 ± 4.6 nm quasi-cube-shaped c-CoO nanocrystals. Method 2: A green slurry of $Co(acac)_3$ (0.20 g, 0.56 mmol) in benzylamine (3.01 g, 28.1 mmol, 50 equiv) and o-dichlorobenzene-(8.25 g, 56.1 mmol, 100 equiv) (1:2 molar ratio of benzylamine: o-dichlorobenzene) was vigorously stirred in a preheated oil bath at 185 °C for 2.5 h to give 8 ± 2 nm c-CoO nanocrystals after a similar purification procedure to that previously listed.

Oxidation of CoO Nanocrystals. h-CoO or c-CoO nanocrystals were loaded in alumina boats in a tube furnace and were annealed at 240 °C for 5 h under an atmospheric pressure of air to yield Co_3O_4 nanocrystals.

Characterization. Cobalt oxide nanocrystals were characterized by X-ray diffraction (XRD) (Rigaku D/MAX-RB diffractometer, using graphite-monochromatized Cu Kα radiation at 40 kV and 100 mA), scanning electron microscopy (SEM) (Philips XL30SFEG operated at 10 and 30 kV), and transmission electron microscopy (TEM) (low resolution: Omega EM912 operated at 120 kV; high resolution: Philips F20Tecai operated at 200 kV) with selected area electron diffraction (SAED) patterns, energy-dispersive analyses of X-ray emission (EDX), and electron energy loss spectroscopy (EELS) at KBSI and KAIST.

Electrochemical Measurements. All electrodes were fabricated by mixing each active material (h-CoO, c-CoO, or spinel Co_3O_4 nanocrystals), acetylene black, and polyvinylidene fluoride (PVDF) with a weight ratio of 7:2:1 using *N*-methylpyrrolidone (NMP) as a solvent. The resulting slurries were pasted onto Cu foils and then dried in a vacuum oven at 120 °C for 6 h. After drying, the electrode foils were pressed and then punched into a disk shape of 13 mm in diameter. The electrochemical properties of the prepared electrodes were evaluated using CR2016 coin-type cells assembled in an argon-filled glovebox. Li metal foil was used as a counter electrode and 1 M solution of $LiPF_6$ in ethylene carbonate (EC) and dimethyl carbonate (DMC) (1:1, v/v) was employed as an electrolyte. The cells were charged and discharged galvanostatically between 0.01 and 3.0 V at 30 °C.

Results and Discussion

Syntheses of h-CoO and c-CoO Nanocrystals. Thermal decomposition of $Co(acac)_3$ in benzylamine under an inert atmosphere yielded two different phases of CoO nanocrystals, h-CoO and c-CoO, through kinetic and thermodynamic reaction control, as illustrated in Scheme 1. When a reaction mixture of $Co(acac)_3$ and 200 equiv of benzylamine was quickly heated to 185 °C and refluxed for 2 h, h-CoO nanocrystals with a hexagonal pyramid shape were formed. In contrast, when the reaction mixture was heated at the relatively low temperature of 130 °C for 12 h and then refluxed at 185 °C for 2 h, c-CoO nanocrystals with a shape of a quasi-cube were produced. Figure 1a shows the TEM and SEM (inset) images of h-CoO hexagonal pyramids with

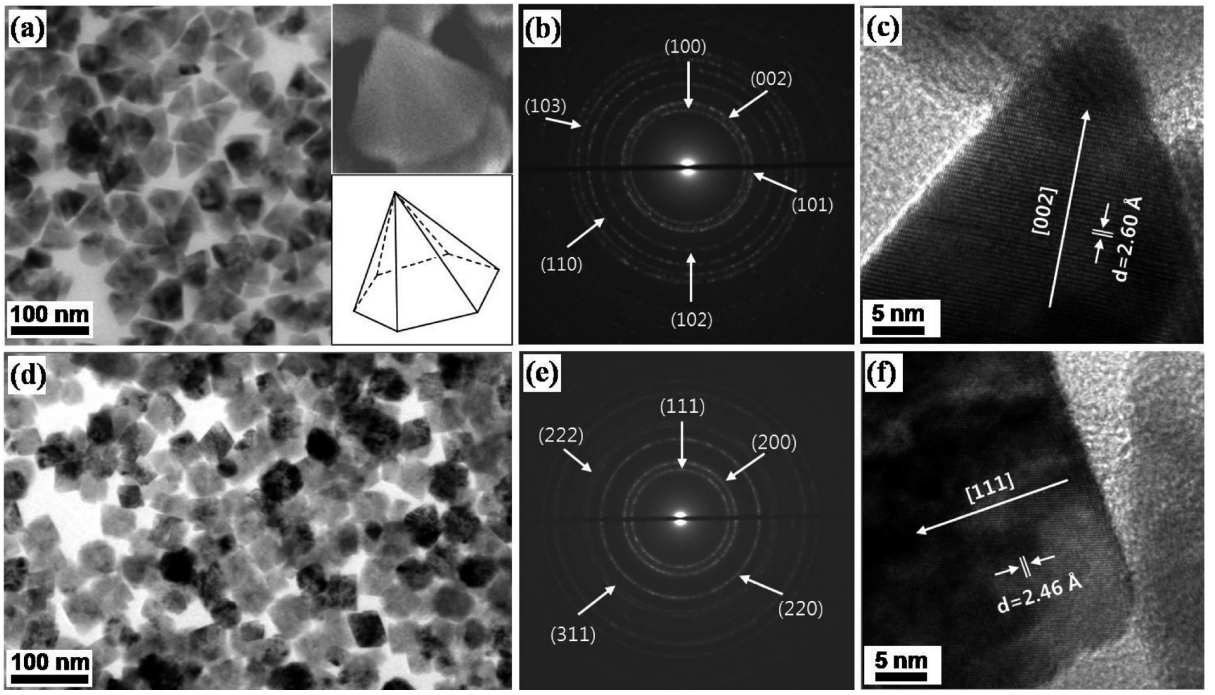

Figure 1. TEM micrographs of CoO nanocrystals: (a) TEM image, (insets) SEM and a schematic diagram, and (b) SAED pattern of h-CoO hexagonal pyramids. (c) HRTEM image of a single h-CoO nanocrystal. (d) TEM image and (e) SAED pattern of c-CoO nanocubes, and (f) HRTEM image of a single c-CoO nanocube.

an average side edge length of 40 ± 6.4 nm. The hexagonal pyramidal shape was confirmed by tilting the hexagon or triangle TEM images (Figure S1 of Supporting Information). The SAED ring patterns are exactly identical to those of the wurtzite CoO phase (Figure 1b).[10] The high resolution TEM (HRTEM) image in Figure 1c reveals that a basal plane of a single h-CoO hexagonal pyramid is (002), and the direction from the base to the top (indicated as a white arrow) is [002]. The lattice spacing corresponding to the (002) plane is estimated to be 2.60 Å. Figure 1d represents that c-CoO nanocrystals have a regular quasi-cube shape with an average edge size of 38 ± 4.6 nm. The SAED patterns clearly show a cubic rocksalt phase of the CoO nanocrystals (Figure 1e). The HRTEM image of an edge in a single c-CoO nanocube shows the lattice spacing of 2.46 Å from (111) planes (Figure 1f). Energy-dispersive X-ray (EDX) spectrometry and electron energy loss spectroscopy (EELS, Figure S2 of Supporting Information) for both h-CoO and c-CoO nanocrystals yielded an average atomic ratio of 49:51 (Co: O), indicative of 1:1 atomic composition.

The detailed reaction mechanism between metal acetylacetonates and benzylamine was previously reported by Niederberger and co-workers.[29] A combined solvolysis-condensation mechanism was proposed: benzylamine attacks to a carbonyl group of the acetylacetonate ligand and aminolysis of acetylacetone involving a C−C bond cleavage results in the formation of *N*-benzylacetamide and enolate ligands, which undergo ketimine condensation reactions to finally induce the formation of metal oxide nanoparticles. Reduction of Co(III) to Co(II) have been explained by dehydrogenative oxidation of benzylamine. This mechanism indicates that amine is indispensable for thermal decomposition of the metal acetylacetonates to produce metal oxides.

We have previously reported the synthesis of metal oxide nanocrystals, such as MnO,[3] Mn_3O_4,[3] and In_2O_3,[30] by using oleylamine not only as a reactant but also as a surfactant. In this work, benzylamine is used as a reactant to finally produce surface-active nanocrystals. Cobaltous oxide nanocrystals synthesized by employing benzylamine have revealed their characteristic electrochemical properties (vide infra), whereas those prepared with oleylamine have not shown any electrochemical activities toward lithium. It seems that most of benzylamine weakly coordinated on the surface of nanocrystals were easily removed during washing and drying processes because of the absence of a long hydrocarbon chain contained in oleylamine.[29,31]

Energetics of CoO Nanocrystals: Kinetic versus Thermodynamic Control. The energetics in different crystallographic phases of materials has been of long-lasting interest.[32−35] Of particular interest is the interplay between rocksalt structure with an octahedral coordination and wurtzite or zinc blende structure with a tetrahedral coordination. The rocksalt MgO is known to be more stable than the wurtzite MgO phase by 0.62 eV/pair in total

(29) Pinna, N.; Garnweitner, G.; Antonietti, M.; Niederberger, M. *J. Am. Chem. Soc.* **2005**, *127*, 5608–5612.
(30) Seo, W. S.; Jo, H. H.; Lee, K.; Park, J. T. *Adv. Mater.* **2003**, *15*, 795–797.
(31) Pinna, N.; Niederberger, M. *Angew. Chem., Int. Ed.* **2008**, *47*, 5292–5304.
(32) Chelikowsky, J. R.; Burdett, J. K. *Phys. Rev. Lett.* **1986**, *56*, 961–964.
(33) Limpijumnong, S.; Lambrecht, W. R. L. *Phys. Rev. B* **2001**, *63*, 104103.
(34) Limpijumnong, S.; Jungthawan, S. *Phys. Rev. B* **2004**, *70*, 054104.
(35) Kung, H. H. *J. Solid State Chem.* **1984**, *52*, 191–196.

lattice energy.[33] However, the wurtzite ZnO is reported to be energetically more stable than the rocksalt ZnO by 0.21 eV/pair.[34] Although c-CoO is more stable than h-CoO by 0.27 eV/pair,[14] interestingly, this work reveals that CoO exists as both rocksalt and wurtzite structures at ambient conditions.

A prolonged heating at a relatively low temperature (130 °C) has yielded c-CoO nanocrystals, whereas a rapid heating of the reaction mixture at refluxing temperature (185 °C) has produced h-CoO nanocrystals, as shown in Scheme 1. In general, when two reaction pathways are plausible from the starting materials, the route with a lower activation barrier affords products faster than the other route, although these products are energetically less stable than those produced via the other route. In this type of reaction, the kinetically controlled reaction generates less stable products, while the thermodynamically controlled reaction yields more stable products. This fundamental concept explains the selective formation of h-CoO and c-CoO nanocrystals by changing the reaction kinetics: flash heating of the reaction mixture provides a kinetically controlled condition to generate the h-CoO nanocrystals, whereas slow and prolonged heating of a thermodynamically controlled condition yields the c-CoO nanocrystals. The crystal structure and morphology of the thermodynamically less stable h-CoO nanocrystals, nevertheless, have been retained under a harsh condition in dioctyl ether at 250 °C for more than 24 h (Figure S3 of Supporting Information). The temperature and pressure for hexagonal-to-cubic phase transformation was reported to be more than 378 °C and 0.8−6.9 GPa, respectively, indicating high stability of the h-CoO nanocrystals.[18,36]

Effect of o-Dichlorobenzene: Formation of h-CoO Nanorods with Various Aspect Ratios and c-CoO Nanocrystals. Selective phase control of CoO has been achieved not only by distinct thermal treatments but also by adding different amounts of o-dichlorobenzene (o-DCB) into the reaction mixture. An addition of o-DCB has altered the particle morphology of h-CoO from hexagonal pyramids to a pencil type of rods with various aspect ratios, which finally transforms into the c-CoO nanocrystals, as described in Scheme 1.

When 20 equiv of o-DCB and 100 equiv of benzylamine with respect to the cobalt precursor concentration were used in the kinetically controlled reaction, nanorods with an average dimension of 11 nm (diameter) × 40 nm (length) were produced (Figure 2a). An increase of the amount of o-DCB to 50 and 80 equiv yielded thin nanorods with dimensions of 9 nm ×50 and 7 nm ×65 nm, respectively (Figure 2b and 2c). The XRD patterns show that all nanorods are composed of h-CoO (vide infra). The HRTEM image of a single nanorod reveals that the rod is single crystalline, and is grown along the unique *c* axis of the h-CoO crystal structure (Figure 2d), where such growth along the *c* axis is an intrinsic nature of the wurtzite structures.[37−39] Further addition of o-DCB to the reaction mixture produced a mixture of h-CoO and c-CoO phases with irregular shapes. When the molar ratio of o-DCB/benzylamine increased to more than 2, c-CoO nanocrystals with an average diameter of 8 nm were obtained (Figure S4 of Supporting Information). On the contrary, an addition of o-DCB under the thermodynamically controlled reaction at a low temperature of 130 °C did not alter the formation of c-CoO nanocrystals.

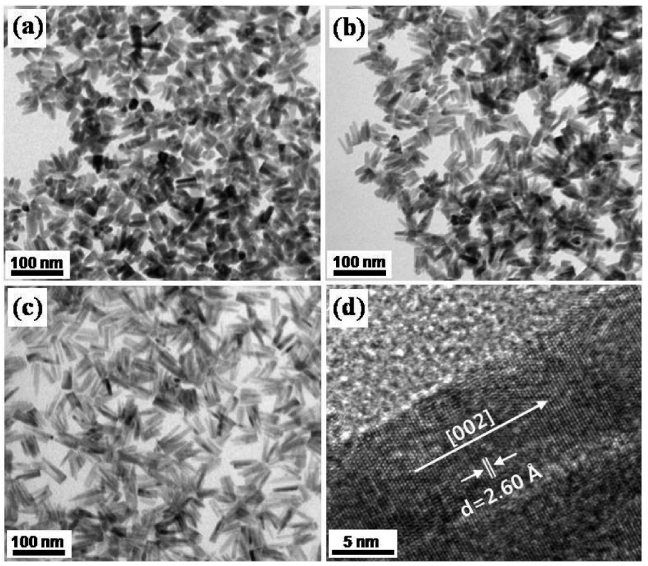

Figure 2. (a, b, c) TEM images and (d) HRTEM image of a h-CoO nanorod with average dimensions of 11 nm ×40 nm (a), 9 nm ×50 nm (b), and 7 nm ×65 nm (c, d).

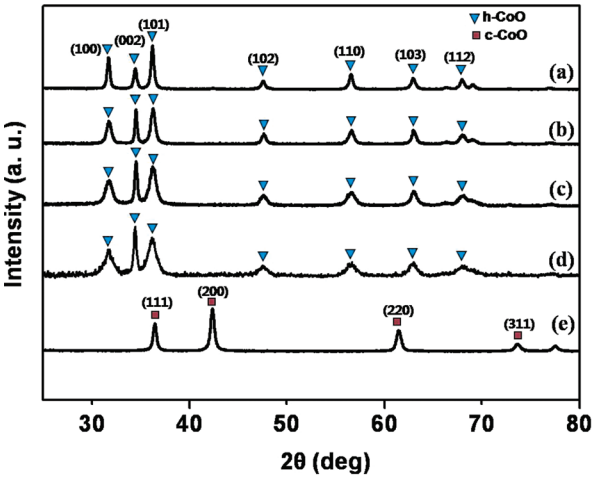

Figure 3. XRD patterns of (a) h-CoO hexagonal pyramids, h-CoO nanorods with the dimensions of (b) 11 nm ×40 nm, (c) 9 nm ×50 nm, and (d) 7 nm ×65 nm, and (e) c-CoO nanocubes.

The XRD patterns of the h-CoO nanorods with various aspect ratios and c-CoO nanoparticles are shown in Figure 3. The diffraction peaks of h-CoO (Figure 3a−d) and c-CoO nanocrystals (Figure 3e) have been indexed to the hexagonal wurtzite CoO (space group: $P6_3mc$) and

(36) Liu, J. F.; He, Y.; Chen, W.; Zhang, G. Q.; Zeng, Y. W.; Kikegawa, T.; Jiang, J. Z. *J. Phys. Chem. C.* **2007**, *111*, 2–5.
(37) Peng, X.; Manna, L.; Yang, W.; Wickham, J.; Scher, E.; Kadavanich, A.; Alivisatos, A. P. *Nature* **2000**, *404*, 59–61.
(38) Pacholski, C.; Kornowski, A.; Weller, H. *Angew. Chem., Int. Ed.* **2002**, *41*, 1188–1191.
(39) He, J. H.; Ho, C. H.; Wang, C. W.; Ding, Y.; Chen, L. J.; Wang, Z. L. *Cryst. Growth Des.* **2009**, *9*, 17–19.

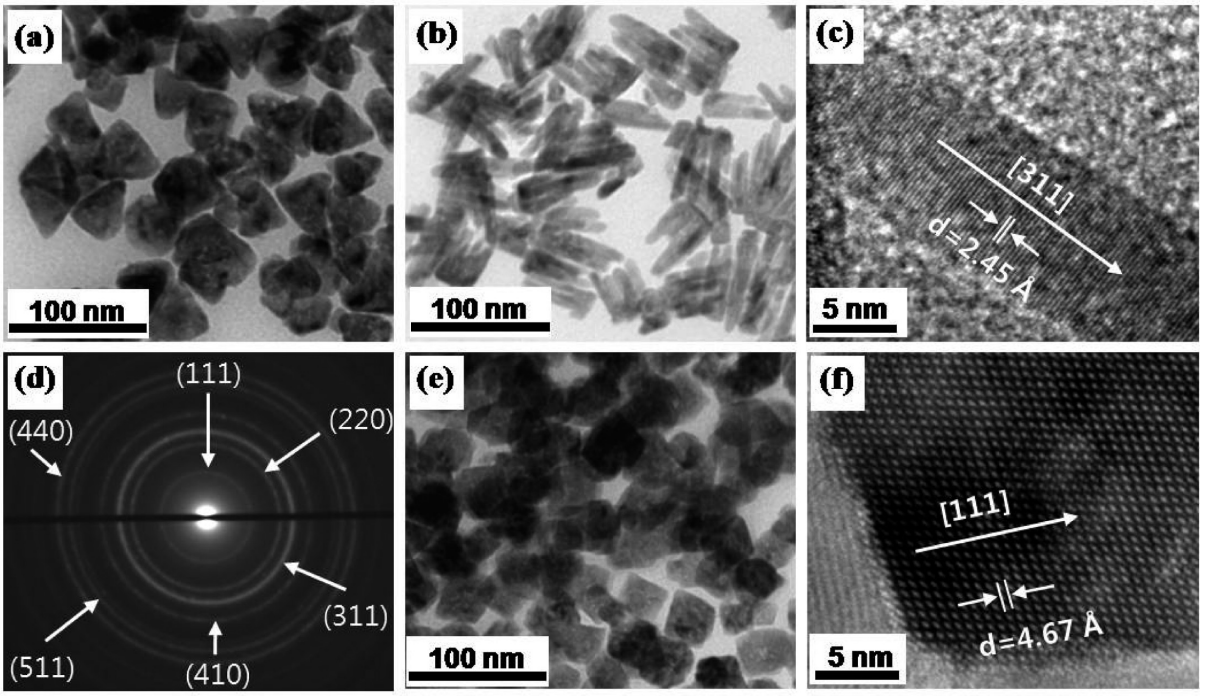

Figure 4. TEM micrographs and SAED pattern of spinel Co_3O_4 nanocrystals: (a) TEM image of Co_3O_4 hexagonal pyramids. (b) TEM and (c) HRTEM images, and (d) SAED pattern of Co_3O_4 nanorods with a dimension of 7 nm ×65 nm. (e) TEM and (f) HRTEM images of Co_3O_4 nanocubes.

cubic rocksalt CoO (space group: *Fm*3*m*) phases, respectively. In h-CoO nanorods, as the aspect ratio increases from 3.6 (11 nm ×40 nm) to 9.3 (7 nm ×65 nm), the (002) peak is sharpened, which coincides with their growth direction along [002]. The intense (002) ring pattern of the nanorods in SAED also matches the [002] growth direction of the nanorods (Figure S5 of Supporting Information).

It is known that a thermodynamically controlled condition generally enhances the growth rate along the *c*-axis in wurtzite crystal structures, and thus generates anisotropic nanorods.[37,38] Hyeon and co-workers reported synthesis of h-CoO nanorods under a thermodynamically controlled condition by decreasing a heating rate.[16] In the present study, instead of changing thermal conditions, the addition of o-DCB led to the elongation of the original morphology. The kinetically controlled condition with flash heating at 185 °C was gradually changed to the thermodynamically controlled condition by the o-DCB addition. When a large amount of o-DCB was added to the reaction mixture, the reaction condition was totally converted to the thermodynamically controlled regime, and consequently the reaction yielded thermodynamically stable c-CoO nanoparticles. It is noteworthy that o-DCB most effectively influences the reaction kinetics and the corresponding products among various high boiling point solvents examined such as octadecene, phenyl ether, and benzyl alcohol. This result is, probably, due to not only dilution of amine by the addition of o-DCB but also more active involvement of o-DCB in the thermal decomposition kinetics of the precursors.

During the synthesis of h-CoO nanocrystals in kinetically controlled reaction at 185 °C, the color of the reaction mixture turned from the green color of the cobalt precursor to the red color of cobalt intermediate species, and finally to the green color of h-CoO nanocrystals. This color change of the reaction mixture is a good indicator of the progress of the reaction. As the amount of o-DCB increased, the color change from red to green slowly proceeded, implying that the formation of h-CoO seeds was significantly slowed down. The effect of o-DCB for the formation of nanorods was examined as well. When a mixture of $Co(acac)_3$ and benzylamine was stirred at 185 °C for 30 min, h-CoO nanoparticles with a diameter of about 8 nm were obtained. o-DCB was added to the reaction mixture at 185 °C, and additionally stirred at the same temperature for 2 h. The final product was formed as h-CoO nanorods with a dimension of 12 nm ×35 nm (Figure S6 of Supporting Information). These results indicate that o-DCB delayed not only the formation of seeds but also crystal growth from the initial seeds during the reaction to form more thermodynamically stable nanorods.

Direct Oxidation of CoO to Co_3O_4 Nanocrystals: Structural Relations among Cobalt Oxide Phases. Direct oxidation of the cobaltous oxide nanocrystals yields spinel Co_3O_4 nanocrystals. The h-CoO and c-CoO nanocrystal powders were loaded on alumina boats, and heated at 240 °C for 5 h under air. Oxidation of h-CoO yielded Co_3O_4 nanocrystals with the shape identical to the original one of the hexagonal pyramid (Figure 4a). The h-CoO nanorods with the dimension of 7 nm ×65 nm were oxidized to yield Co_3O_4 nanorods also with retention of their morphology (Figure 4b). The HRTEM image in Figure 4c shows the lattice spacing of 2.45 Å from the adjacent (311) planes of spinel Co_3O_4, and the SAED pattern corresponds to the

spinel Co_3O_4 phase (Figure 4d).[40] The Co_3O_4 nanocubes were obtained by oxidation of the c-CoO nanocubes (Figure 4e). Figure 4f shows an edge of a single nanocrystal with the lattice spacing of 4.67 Å from the (111) planes of Co_3O_4, and the SAED pattern is assigned as spinel Co_3O_4 (Figure S7 of Supporting Information). EDX and EELS data (Figure S8 of Supporting Information) for both Co_3O_4 hexagonal pyramids and Co_3O_4 nanocubes clearly demonstrate the stoichiometric compositions of O/Co $\approx$ 4:3. Remarkably, all the nanocrystals produced maintain their morphology during oxidation under such harsh conditions. Theoretically, about 8% of volume decrease for the transformation of h-CoO (density (d) = 5.23 g/cm^3) and about 14% of volume increase for the transformation of c-CoO (d = 6.44 g/cm^3) to spinel Co_3O_4 (d = 6.06 g/cm^3) would be expected to be observed. However, such significant volume changes were not detected in the TEM data (Figure 1 and 4), and the single crystalline features were maintained over all Co_3O_4 nanostructures.

To understand the structural relation between the CoO and Co_3O_4 phases, the HRTEM images and corresponding lattice structures were carefully examined. In the conversion of c-CoO to spinel Co_3O_4, the lattice fringe image of the c-CoO nanocube corresponds to that of the spinel Co_3O_4 nanocube (Figure S9 of Supporting Information). The (111) lattice planes are parallel to the edges of both nanocubes, although the lattice spacings between neighboring planes are quite distinct. The simulation of the lattice structures shows a close relation between c-CoO and spinel Co_3O_4 phases (Figure S9 of Supporting Information). The lattice arrangements in a view along the [111] direction indicate that both phases have identical positions of oxygen atoms. Langell et al. reported the epitaxial relation between the (100) planes of spinel Co_3O_4 and those of c-CoO in a single crystalline thin film.[41] In this epitaxial Co_3O_4 formation on the c-CoO surface under oxidizing conditions, the cobalt cations (Co^{2+}) moved from the octahedral sites of the c-CoO phase to half of the octahedral sites (as a form of Co^{3+}) and one-eighth of the tetrahedral sites (as a form of Co^{2+}) of the spinel Co_3O_4, while the oxygen lattice with cubic close-packed arrangement has been retained.[41] However, in the conversion of h-CoO to spinel Co_3O_4 nanocrystals, there are no planes of spinel Co_3O_4 corresponding to the planes of the h-CoO phase. The (311) lattice planes of the Co_3O_4 nanorod in Figure 4c are not exactly orthogonal to the growth direction of the Co_3O_4 nanorod, in contrast to the case of the (002) lattice planes of h-CoO nanocrystals. Because of this lattice mismatch between h-CoO and Co_3O_4, oxidation has not occurred in an epitaxial fashion, but formed polycrystalline domains at an intermediate stage of the reaction during conversion of h-CoO to Co_3O_4 (vide infra, Figure S10a of Supporting Information).

Progress of the Oxidation Reactions and Simultaneous Phase Conversion. The progress of the oxidation reactions has been monitored at a regular reaction period by XRD. The oxidation reaction of h-CoO (XRD spectrum: Figure 5a) has been examined at 240 °C for 10 min (Figure 5b), 20 min (Figure 5c), and 5 h (Figure 5d). Figures 5a and 5d show typical XRD patterns of h-CoO and spinel Co_3O_4 phases, respectively. Interestingly, the (200) and (220) peaks of c-CoO (marked as ■) appear, as well as the h-CoO (▼) and Co_3O_4 (●) peaks in Figure 5b, 5c, and S11 of Supporting Information, indicating that the conversion from h-CoO to c-CoO takes place rapidly as the oxidation reaction proceeds. The formation of c-CoO and Co_3O_4 has been observed within 10 min, and the starting h-CoO has been completely consumed within 20 min after oxidation in air. The HRTEM image of h-CoO nanocrystals after oxidation for 10 min demonstrates the polycrystalline nature of the sample involving a number of small crystalline domains in the nanocrystal (Figure S10a of Supporting Information). The high temperature annealing for 5 h improves crystallinity of the nanoparticles (Figure 5d). This is reasonable because the cobalt cations and oxygen anions of h-CoO must totally rearrange their positions to the new lattice points of the spinel Co_3O_4 phase.

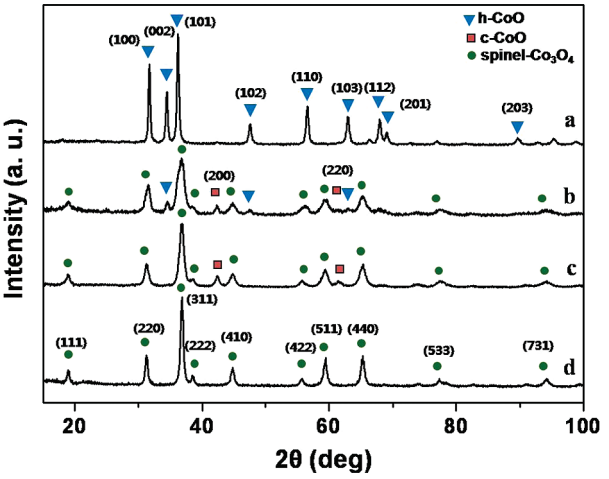

Figure 5. XRD spectra of h-CoO hexagonal pyramids: (a) before and after heat treatment at 240 °C for (b) 10 min, (c) 20 min, and (d) 5 h in air.

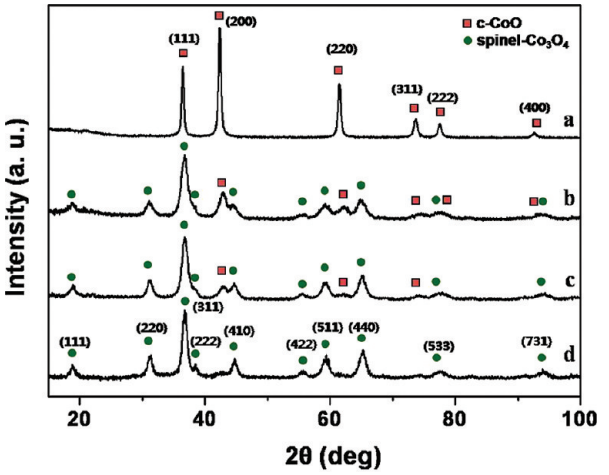

Figure 6. XRD spectra of c-CoO nanocubes: (a) before and after heat treatment at 240 °C for (b) 10 min, (c) 20 min, and (d) 5 h in air.

(40) Nethravathi, C.; Sen, S.; Ravishankar, N.; Rajamathi, M.; Pietzonka, C.; Harbrecht, B. *J. Phys. Chem. B* **2005**, *109*, 11468–11472.
(41) Langell, M. A.; Anderson, M. D.; Carson, G. A.; Peng, L.; Smith, S. *Phys. Rev. B* **1999**, *59*, 4791–4798.

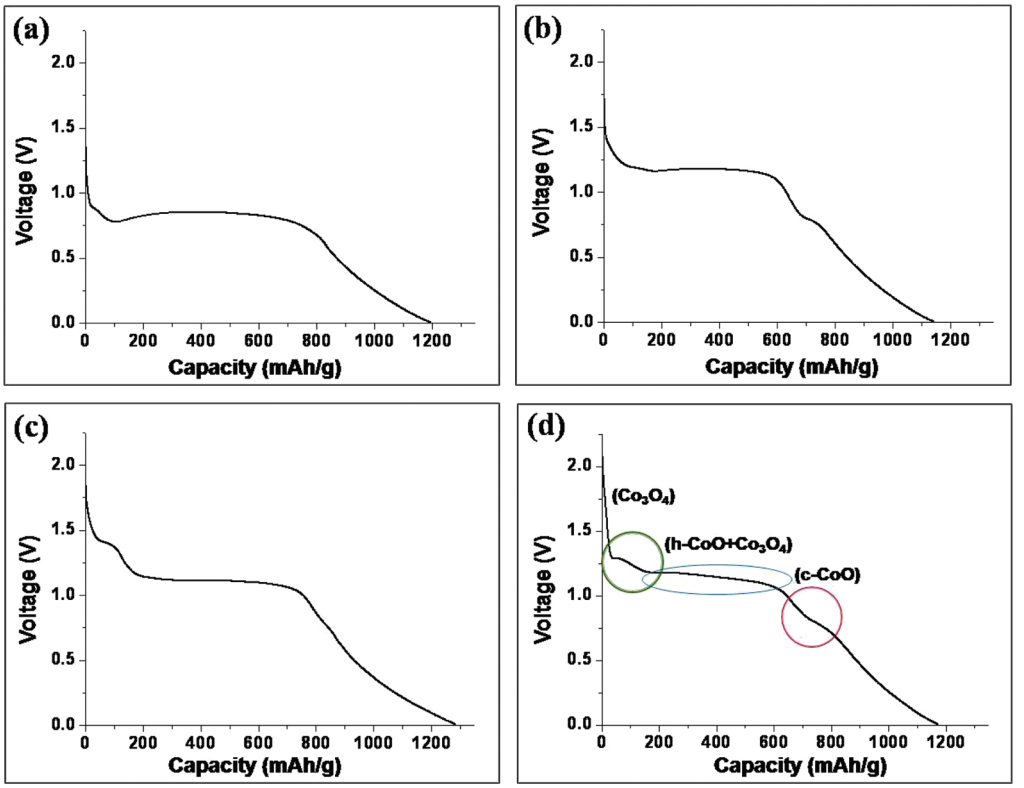

Figure 7. First discharge graphs of (a) c-CoO, (b) h-CoO, and (c) spinel Co_3O_4 nanocrystals, and (d) a sample of h-CoO hexagonal pyramids after heating at 240 °C for 10 min in air.

The c-CoO nanocubes (XRD spectrum: Figure 6a) have also been oxidized in air at a similar oxidation condition and monitored for 10 min (Figure 6b), 20 min (Figure 6c), and 5 h (Figure 6d). The oxidation reaction for 5 h yields pure spinel Co_3O_4 nanocrystals. It is notable that single crystalline features of the nanocrystals have been maintained throughout the oxidation process. Figure S10b of Supporting Information shows that the lattice fringe images are continuous over the entire crystal, although the main fraction is already oxidized to form Co_3O_4. The movement of cobalt cations transforms the crystal structure without breaking single crystallinity, since the c-CoO and spinel Co_3O_4 phases are epitaxial with an identical cubic close-packed arrangement of the oxygen lattice. It should be noted that this cation rearrangement takes 5 h to complete the oxidation, implying that deeply buried cobalt cations are difficult to move to other positions because of strict confinement of the crystal structure.

By monitoring the oxidation reactions of the h-CoO and c-CoO nanocrystals to form Co_3O_4, the rearrangements of the cobalt cations and oxygen anions during the oxidation process have been clearly understood. The movement of the cobalt cations in the center of the c-CoO nanoparticles takes 5 h, whereas the oxygen rearrangement in the h-CoO nanocrystals to form c-CoO and Co_3O_4 takes place within 20 min. Consequently, the simultaneous conversion of h-CoO to c-CoO during oxidation can be elucidated by these distinct rearrangement rates between the cobalt cations and the oxygen lattice. The rearrangement of the oxygen lattice is relatively fast to form the cubic closed-packed array under the oxidation condition, but the buried cobalt cations at the center of the particles are too slow to occupy the new positions in the spinel Co_3O_4 structure, resulting in the formation of the c-CoO intermediate phase. The conversion of c-CoO to Co_3O_4 is still slow enough to be detected by XRD. Slow oxidation of the h-CoO nanocrystals by prolonged heating at a low temperature of 180 °C does not generate the c-CoO phase, but directly produces the spinel Co_3O_4. This implies that the rearrangement of the oxygen lattice was not much faster than the movement of the Co cations in this low temperature reaction condition.

Another interesting point in the oxidation experiment is that the XRD peaks of the c-CoO phase in Figure 6b are slightly shifted to higher angles by 0.75° (Figure S12 of Supporting Information). It has been recently reported that the XRD peaks of c-CoO nanocrystals were shifted to higher angles under a high pressure.[36,42] In our crystal system, fast oxidation of c-CoO nanocrystals has led to the formation of Co_3O_4 without increasing the volume of the nanocrystals at the initial stage of the oxidation, which causes the c-CoO phase to be pressurized enough to shift the XRD signals to higher angles.

Electrochemical Properties of Cobalt Oxide Nanocrystals toward Lithium. The electrochemical properties of the three different cobalt oxide nanocrystals of c-CoO, h-CoO, and spinel Co_3O_4 have been investigated by assembling Li/cobalt oxides half-cells, and the results are shown in Figure 7. The first discharge curve of the c-CoO

(42) Guo, Q.; Mao, H.-K.; Hu, J.; Shu, J.; Hemley, R. J. *J. Phys.: Condens. Matter* **2002**, *14*, 11369–11374.

nanocrystals (Figure 7a) shows a characteristic feature observed for the rocksalt CoO phase with a well-defined potential plateau at 0.8 V versus Li^+/Li, which is attributed to the reduction of c-CoO to metallic Co.[23] The electrochemical feature of the h-CoO nanocrystals is unprecedented. The first discharge graph of h-CoO exhibits a potential plateau of 1.2 V (Figure 7b). The potentials of electrode materials during the reaction with lithium are known to be closely related to Gibbs free energies of their electrochemical reactions. Therefore, the difference of 0.4 V between the potential plateaus of c-CoO and h-CoO is attributed to apparent disparity in their reaction free energies. The local structure of c-CoO is composed of CoO_6 octahedra, whereas that of h-CoO is CoO_4 tetrahedra. The crystal field stabilization energy (CFSE) for octrahedral coordination is larger than that for tetrahedral coordination in weak field d^7 (Co^{2+}) oxides. This explains why the reduction to Co of h-CoO is much easier than that of c-CoO. Another interesting feature of this first discharge in h-CoO nanocrystals is that a shoulder is observed at a potential ~0.8 eV, identical to the potential plateau of c-CoO. This implies that part of the h-CoO nanocrystals are initially converted to c-CoO during the reduction process, and the resulting c-CoO phase is in turn reduced to Co at 0.8 eV.

The first discharge curve of the spinel Co_3O_4 shows characteristic features observed in spinel Co_3O_4 with two well-defined voltage plateaus at around 1.3 and 1.1 V (Figure 7c): the high voltage plateau at ~1.3 V is attributed to the formation of small c-CoO clusters, which were normally observed for the nanostructured spinel Co_3O_4 with high surface area or at very low current density.[24] The main reduction plateau at ~1.1 V is related to the transformation of partially lithiated cobalt oxides ($Li_xCo_3O_4$) into metallic Co.[24,43] To assign the plateaus in each phase, the h-CoO has been heated at 240 °C in air for 10 min, where the resulting nanocrystals should contain three cobalt oxide phases of h-CoO, c-CoO, and spinel Co_3O_4 as described above. As expected, the first discharge graph of this sample clearly exhibits three distinct plateaus (Figure 7d). The plateaus at ~1.3 V, 1.1−1.2 V, and ~0.8 V versus Li^+/Li are due to the spinel Co_3O_4, the mixture of h-CoO and spinel Co_3O_4, and the c-CoO phase, respectively. It is notable that the electrochemical measurement toward lithium is one of the potential methods to identify distinct metal oxide phases in nanostructured crystals. We are currently studying the detailed electrochemical properties and redox mechanisms of the CoO nanocrystals as negative electrode materials for lithium ion batteries.

(43) Thackeray, M. M.; Baker, S. D.; Adendorff, K. T.; Goodenough, J. B. *Solid State Ionics* **1985**, *17*, 175–181.

Conclusion

We have demonstrated the facile synthesis of h-CoO and c-CoO nanocrystals by thermal decomposition of $Co(acac)_3$ in the presence of benzylamine. The phase and morphology of the CoO nanocrystals are manipulated by controlling thermal decomposition kinetics, such as employing different heating conditions and adding o-DCB to the reaction mixture. Kinetically controlled reaction with flash heating at high temperature yields h-CoO hexagonal pyramids, whereas thermodynamically controlled reaction with prolonged heating at a low temperature produces c-CoO nanocubes, selectively. Interestingly, the product has been altered from h-CoO hexagonal pyramids to h-CoO nanorods with various aspect ratios and finally c-CoO nanocrystals by addition of o-DCB under the kinetically controlled condition. The spinel Co_3O_4 nanocrystals with the shape of hexagonal pyramids, rods, and cubes have been successfully formed by air oxidation of the h-CoO and c-CoO nanocrystals with retention of their original morphology. The three distinct cobalt oxide nanocrystals of h-CoO, c-CoO, and spinel Co_3O_4 phases have been found to exhibit characteristic electrochemical properties toward lithium. Our results allow preparation of selectively pure h-CoO, c-CoO, and spinel Co_3O_4, understanding the detailed mechanisms and energetics of the formation and oxidation of these cobalt oxide nanocrystals with various crystal phases and morphlogies, and open up the possibility of tuning electrochemical properties using a rational control of the metal oxide structures.

Acknowledgment. This work was supported by the Korea Research Foundation Grant funded by the Korean Government (MOEHRD) (KRF-2005-201-C00021) and by the Nano R&D program (Grant 2005-02618) of the Korea Science and Engineering Foundation (KOSEF) funded by Korean Ministry of Science & Technology (MOST). This work was supported by National Research Foundation of Korea Grant funded by the Korean Government (20090063004). W.S.S. also acknowledges the financial support from the National Research Foundation of Korea Grant funded by the Korean Government (KRF-2008-331-C00147) and the Sogang University Research Grant of 2007. We thank KBSI and KAIST for the TEM analyses.

Supporting Information Available: TEM and HRTEM images, EELS, XRD patterns, SAED patterns, and lattice simulation results for three different cobalt oxide nanocrystals with h-CoO hexagonal pyramids and rods, c-CoO cubes, and Co_3O_4 nanocrystals. This material is available free of charge via the Internet at http://pubs.acs.org.